Research Square

Preprints are preliminary reports that have not undergone peer review.
They should not be considered conclusive, used to inform clinical practice,
or referenced by the media as validated information.

Basal Ganglia Iron Accumulation Mediates Stage-Dependent Associations Between Plasma pTau217 and Hippocampal Atrophy in Alzheimer's Disease

Pengbo Gao
Affiliated Brain Hospital of Guangzhou Medical University
Haoye Tan
Affiliated Brain Hospital of Guangzhou Medical University
Guangshi Li
Affiliated Brain Hospital of Guangzhou Medical University
Jinxia Liang
Affiliated Brain Hospital of Guangzhou Medical University
Mingfeng Yang
Affiliated Brain Hospital of Guangzhou Medical University
Danyan Xu
Affiliated Brain Hospital of Guangzhou Medical University
Qiang Wang
Affiliated Brain Hospital of Guangzhou Medical University
Shuang Liang
Affiliated Brain Hospital of Guangzhou Medical University
Zhidai Xiao
Affiliated Brain Hospital of Guangzhou Medical University
Xiaomin Zheng
Affiliated Brain Hospital of Guangzhou Medical University
Yujiing Gan
Affiliated Brain Hospital of Guangzhou Medical University
Qixuan Chen
Affiliated Brain Hospital of Guangzhou Medical University
Mingyong Zeng
Affiliated Brain Hospital of Guangzhou Medical University
Weilin Wang
Affiliated Brain Hospital of Guangzhou Medical University
Ben Chen
Affiliated Brain Hospital of Guangzhou Medical University
Xiaomei Zhong

Affiliated Brain Hospital of Guangzhou Medical University

Yuping Ning

ningjeny@126.com

Affiliated Brain Hospital of Guangzhou Medical University

Research Article

Keywords: Alzheimer's disease, pTau217, iron deposition, hippocampus, cognitive decline, quantitative susceptibility mapping.

Posted Date: October 19th, 2026

DOI: https://doi.org/10.21203/rs.3.rs-11017150/v1

License: This work is licensed under a Creative Commons Attribution 4.0 International License. Read Full License

Additional Declarations: No competing interests reported.

Abstract

Background

Plasma phosphorylated tau 217 (pTau217) reflects cerebral tau pathology in Alzheimer's disease (AD), yet how brain iron deposition mediates the relationship between pTau217 and hippocampal atrophy across AD stages remains unknown.

Methods

193 participants were classified as AD (n = 94) or Non-AD (n = 99) based on a plasma pTau217 threshold of 0.242 pg/mL, and AD individuals were further staged as preclinical AD, prodromal AD, or AD dementia. All underwent plasma biomarker profiling, quantitative susceptibility mapping (QSM), structural MRI, and neuropsychological assessment. Stage-dependent, iron-stratified, and mediation and cutoff-sensitivity analyses were performed.

Results

AD individuals showed increased iron deposition in the basal ganglia, predominantly the putamen, and reduced bilateral hippocampal volumes. Basal ganglia iron correlated positively with pTau217 and inversely with global cognition, episodic memory, language, and visuospatial function (all $pFDR < 0.05$). Iron–hippocampus associations strengthened progressively across the continuum, peaked in prodromal AD, and plateaued in dementia, and iron burden modified the pTau217–hippocampus slope. Basal ganglia iron partially mediated the pTau217–hippocampal volume relationship bilaterally (both $p < 0.05$), accounting for 6.4% to 7.9% of the total effect.

Conclusion

Basal ganglia iron serves as a stage-dependent mediator linking pTau217 to hippocampal neurodegeneration, with prodromal AD potentially indicating a particularly vulnerable stage for iron-targeted interventions and iron profiling for patient stratification.

1. Background

Alzheimer's disease (AD) is characterized by a prolonged preclinical phase during which neuropathological changes accumulate years before clinical symptoms emerge. Early and accurate identification of individuals on the AD trajectory remains a critical challenge for implementing disease-modifying interventions during the therapeutic window. Recent advances in ultrasensitive immunoassays have positioned plasma phosphorylated tau at threonine 217 (pTau217) as a highly specific and accessible biomarker that reflects cerebral amyloid-β and tau pathology with remarkable fidelity,

outperforming other plasma tau species in discriminating AD from other neurodegenerative disorders[1–3]. Notably, elevated plasma pTau217 has been strongly associated with hippocampal atrophy, a hallmark of AD neurodegeneration. However, the intermediate pathophysiological mechanisms linking pTau217-indexed pathology to regional brain atrophy and cognitive decline remain incompletely understood, particularly regarding modifiable processes that may represent therapeutic targets.

Brain iron dysregulation has emerged as a compelling intermediate mechanism linking tau pathology to neurodegeneration. Iron accumulates preferentially in the basal ganglia during normal aging, and this accumulation is markedly accelerated in AD[4–6]. The basal ganglia are particularly vulnerable due to their high metabolic demands and dense dopaminergic innervation, and their extensive reciprocal projections with hippocampal-entorhinal circuits suggest that subcortical iron-induced dysfunction may propagate to and exacerbate tau-mediated degeneration in medial temporal structures[7]. Iron may also interact directly with tau pathology within the basal ganglia, where iron-catalyzed oxidative stress promotes tau hyperphosphorylation and aggregation, potentially accelerating transsynaptic tau spread to connected hippocampal regions[8]. At the molecular level, iron catalyzes the generation of reactive oxygen species through Fenton chemistry, promotes tau hyperphosphorylation and aggregation via activation of glycogen synthase kinase-3β, and triggers ferroptosis, an iron-dependent form of regulated cell death increasingly implicated in neurodegeneration[8–11]. Quantitative susceptibility mapping (QSM) enables non-invasive quantification of brain iron content, providing a tool to examine whether regional iron accumulation mediates the relationship between peripheral tau burden and central structural brain changes in AD.

Understanding how iron-related neurodegeneration varies across AD stages is crucial for identifying therapeutic windows. Prior research suggests stage-dependent variability in the relationship between iron accumulation and neurodegeneration, yet systematic examination across the AD continuum remains limited[12, 13]. Systematically examining these stage-dependent and individual-level variations is essential for determining when iron dysregulation becomes a critical driver of hippocampal atrophy and identifying optimal therapeutic windows for iron-targeted interventions. The hippocampus, showing progressive atrophy paralleling cognitive decline and tau pathology[15, 16], is particularly vulnerable in AD. The basal ganglia and hippocampus are interconnected through cortico-striatal-hippocampal circuits, such that iron-induced subcortical damage may propagate to medial temporal structures[17, 18]. Moreover, the hippocampus itself is susceptible to iron accumulation and oxidative stress, though the relative contributions of local versus network-mediated iron effects remain unclear[19, 20]. Examining whether basal ganglia iron mediates the relationship between plasma tau biomarkers and hippocampal degeneration could illuminate a critical pathophysiological pathway amenable to therapeutic intervention.

Despite these converging lines of evidence, no study has systematically examined how the interrelationships among plasma pTau217, basal ganglia iron deposition, and hippocampal atrophy evolve across AD clinical stages or vary according to individual iron burden. Constructing a more complete pathophysiological model that integrates accessible peripheral biomarkers with specific

central nervous system changes across disease stages is essential. Such an integrative approach may identify novel intervention targets, refine patient stratification for clinical trials, and inform the development of personalized therapeutic strategies based on individual iron homeostasis profiles.

To address these gaps, we conducted a comprehensive study combining plasma biomarker profiling, QSM-based iron quantification, structural neuroimaging, and neuropsychological evaluation in a cohort stratified by pTau217 status. We aimed to: (1) characterize differences in basal ganglia iron deposition and hippocampal volumes between AD and Non-AD individuals; (2) examine stage-specific associations among iron deposition, pTau217, and hippocampal volumes across preclinical, prodromal, and dementia stages; (3) investigate how iron levels modulate the relationship between pTau217 and hippocampal atrophy; and (4) determine whether basal ganglia iron mediates the relationship between plasma pTau217 and hippocampal neurodegeneration and cognitive decline through mediation modeling.

2. Methods

2.1. Study participants and design

This cohort comprised 193 individuals aged 50 years or older, recruited from the Affiliated Brain Hospital of Guangzhou Medical University. Eligible participants presented with normal cognition (defined by education-adjusted Mini-Mental State Examination [MMSE] thresholds based on Chinese normative data: >17 for illiterate individuals, > 20 for those with primary education, and > 24 for those with middle school education or higher), mild cognitive impairment (defined by Petersen criteria[21]), or dementia (per DSM-IV diagnostic standards[22]). Individuals were excluded if they had malignancies, significant cerebrovascular events (e.g., stroke or hemorrhage with residual deficits), other major neurological conditions (e.g., encephalitis, multiple sclerosis, epilepsy, traumatic brain injury, or normal pressure hydrocephalus), primary psychiatric disorders (e.g., schizophrenia, bipolar disorder, or intellectual disability), or systemic illnesses known to affect cognition (e.g., hepatic or renal dysfunction, thyroid abnormalities, severe anemia, infectious diseases, or substance abuse). Each participant completed a standardized clinical evaluation, plasma biomarker sampling, and multimodal MRI acquisition.

Plasma pTau217 levels were measured and dichotomized using a threshold of 0.242 pg/mL established in our previous study[23], yielding a AD (pTau217-positive) group (n = 94) and an Non-AD (pTau217-negative) group (n = 99). This threshold was derived by maximizing the Youden index against amyloid status in a research cohort with 18F-florbetapir PET (The Southern China Aging Brain Initiative cohort (SCABI)-1, n = 182) and validated in an independent internal cohort (SCABI-2, n = 78) and an external real-world cohort with amyloid status defined by the FDA-cleared CSF Aβ1–42/Aβ1–40 ratio (n = 100), in which plasma pTau217 achieved an AUC of 0.94–0.96 for amyloid positivity. Details of its derivation, validation, and diagnostic performance are provided in the **Supplementary Material**. The AD group was subsequently categorized into three disease stages: preclinical Alzheimer's disease (cognitively normal individuals with pTau217 positivity), prodromal Alzheimer's disease (those with mild cognitive

impairment and pTau217 positivity), and Alzheimer's disease dementia (individuals meeting dementia criteria with pTau217 positivity)[24]. The overall design and workflow of the study are illustrated in Fig. 1.

2.2. Neuropsychological assessment

All participants completed a standardized battery of neuropsychological tests administered by a certified neuropsychologist. Global cognitive function was assessed using the Mini-Mental State Examination (MMSE) and Clinical Dementia Rating (CDR) scale. Domain-specific cognitive performance was evaluated across five functional areas: memory was assessed using the Auditory Verbal Learning Test (AVLT) including immediate, short-delay, and long-delay recall trials; information processing speed was measured by the Symbol-Digit Modalities Test (SDMT) and Trail Making Test Part A (TMTA); language function was evaluated through the Boston Naming Test (BNT) and Verbal Fluency Test (VFT); executive function was assessed using the Stroop Color and Word Test C (Stroop-C) and Trail Making Test Part B (TMTB); visuospatial ability was measured by the Rey-Osterrieth Complex Figure Test (ROCF).

2.3. Plasma biomarker extraction

Plasma samples were collected in 5 mL polypropylene tubes and processed within 4 hours by centrifugation (2000 × g, 10 min, 4°C). Aliquots of 0.5 mL were stored at -80°C, with only previously unfrozen samples analyzed to prevent degradation. Plasma pTau217 and pTau181 were quantified using the Lumipulse G1200 automated platform (Fujirebio). Additional biomarkers including Aβ40, Aβ42, Aβ42/40 ratio, and neurofilament light chain (NfL) were measured according to manufacturer instructions[23].

2.4. MRI acquisition and processing

All participants underwent multimodal MRI scanning on a 3.0 Tesla Siemens Magnetom Prisma scanner with a 64-channel head coil. High-resolution T1-weighted images were acquired using an MPRAGE sequence (TR = 2000 ms, TE = 2.32 ms, TI = 900 ms, flip angle = 8°, isotropic voxel size = 0.6 mm). Quantitative susceptibility mapping (QSM) data were obtained using a multi-echo gradient echo sequence (TR = 39 ms; TE1 = 3.09 ms, and ΔTE = 4.91 ms; matrix size = 192 × 256 × 144; isotropic voxel size = 1 mm; and flip angle = 15°). Structural images were processed using CAT12 (version 12.8.2)[25] within SPM12 on MATLAB R2021b. Preprocessing included bias-field correction, skull-stripping, tissue segmentation, and spatial normalization to Montreal Neurological Institute (MNI) space via geodesic shooting. Total intracranial volume (TIV) was estimated for head size correction. Regional gray matter volumes were extracted using the AAL3 atlas[26], focusing on bilateral hippocampus as the primary region of interest given its central role in AD-related neurodegeneration. QSM reconstruction used STI Suite (version 3.0, https://people.eecs.berkeley.edu/~chunlei.liu/software.html), involving Laplacian-based phase unwrapping, brain extraction, background field removal via V-SHARP, and susceptibility reconstruction using STAR-QSM. QSM images were co-registered to T1 images and normalized to MNI

space. Susceptibility medians after global referencing were extracted from the clusters, which had significant difference in the whole-brain voxel-wise comparisons, for further analyses.

2.5. Statistical analysis

Statistical analyses were performed using Python (version 3.7.15) and R (version 4.4.1). Group comparisons employed chi-square test for categorical variables and independent samples t-test or Mann-Whitney U test for continuous variables depending on data distribution. Partial correlation analyses examined relationships between basal ganglia iron deposition (the significant clusters in whole-brain comparisons), plasma biomarkers, hippocampal volumes, and cognitive performance, adjusting for age and sex with false discovery rate (FDR) correction. To explore potential interaction effects, participants were stratified by iron level (high vs. low, median split) and disease stage, with interaction analyses examining whether the relationship between pTau217 and hippocampal volumes varied across these strata. Mediation analyses investigated whether basal ganglia iron mediated the relationship between plasma pTau217 and hippocampal atrophy, with age and sex as covariates; the significance of indirect effects was evaluated using bootstrapping with 5,000 resamples and bias-corrected 95% confidence intervals. Statistical significance was set at $p < 0.05$.

To evaluate whether the findings depended on the specific plasma pTau217 threshold adopted, three pre-specified sensitivity analyses were performed. First, we quantified the number of participants falling within a “gray zone” of ± 0.005 to ± 0.100 pg/mL around the published cutoff of 0.242 pg/mL, that is, those whose group assignment would be most vulnerable to measurement error or to a small shift in the threshold. Second, the group differences in basal ganglia iron and in left, right, and total hippocampal volume at the published cutoff were re-examined using both a parametric test (Welch t test) and a non-parametric test (Mann–Whitney U test), with Cohen's d and its 95% confidence interval reported as effect sizes. Third, a cutoff-scanning analysis was conducted in which each of 91 candidate thresholds spanning the observed pTau217 range (0.069–1.418 pg/mL) was used in turn to re-dichotomize the full sample, and the group difference was retested at every candidate value (**details in Supplementary material**).

3. Results

3.1. Demographic, clinical characteristics, and biomarker profiles

Demographic, clinical, and biomarker characteristics are presented in Table 1. The AD group (n = 94) and Non-AD group (n = 99) were comparable in sex distribution (29.8% vs 31.3% male, $p = 0.941$) and age (68.64 ± 8.91 vs 67.05 ± 7.50 years, $p = 0.181$), but differed significantly in education level (9.31 ± 3.87 vs 10.70 ± 3.98 years, $p = 0.009$), and cognitive status distribution ($p < 0.001$). The AD group exhibited significantly elevated plasma pTau217, pTau181, and NfL levels, along with reduced Aβ42 and Aβ42/40 ratio (all $p < 0.001$), while Aβ40 levels were comparable ($p = 0.992$). Additionally, the AD group

demonstrated significantly worse performance across all cognitive domains, including global cognition (MMSE, CDR), memory (AVLT), information processing speed (SDMT, TMTA), executive function (TMTB, Stroop-C), visuospatial function (ROCF), and verbal fluency (VFT) (all $p < 0.01$). When compared with the cognitively unimpaired Non-AD subgroup, the AD group, the differences in plasma biomarkers and cognitive performance were of the same direction and larger magnitude. The comparison between AD participants and cognitively unimpaired Non-AD participants is presented in the **Supplementary Results** and **Table S1**.

Table 1
Demographic, clinical, and biomarker characteristics of participants stratified by pTau217 status

Sex (male %)	**AD**	**Non-AD**	***p value***
	(N = 94)	**(N = 99)**	
	28 (29.8%)	**31 (31.3%)**	**0.941[a]**
Age (years)	68.64(8.91)	67.05 (7.50)	0.181[b]
Education (years)	9.31 (3.87)	10.70 (3.98)	**0.009[c]**
SBP (mmHg)	133.05 (19.38)	127.56 (16.11)	**0.034[b]**
DBP (mmHg)	77.26 (11.54)	76.85 (9.45)	0.788[b]
MBP (mmHg)	95.85 (12.60)	93.75 (10.11)	0.203[b]
Cognitive Status			**< 0.001[c]**
Cognitively Unimpaired	12 (12.8%)	34 (34.3%)	
MCI	40 (42.6%)	52 (52.5%)	
Dementia	42 (44.6%)	13 (13.1%)	
Plasma biomarkers			
pTau217(pg/mL)	0.78 (0.51)	0.13 (0.05)	**< 0.001[c]**
Aβ40(pg/mL)	279.52 (57.02)	276.15 (44.52)	0.992[c]
Aβ42(pg/mL)	24.32 (5.59)	28.09 (5.98)	**< 0.001[c]**
Aβ42/40	0.09 (0.01)	0.10 (0.01)	**< 0.001[c]**
NfL(pg/mL)	29.68 (17.66)	19.27 (8.85)	**< 0.001[c]**
pTau181(pg/mL)	4.13 (1.67)	2.49 (1.12)	**< 0.001[c]**
Global cognitive			
MMSE	17.14 (6.27)	22.43 (5.39)	**< 0.001[c]**
CDR	0.96 (0.66)	0.59 (0.39)	**< 0.001[c]**
Memory			
AVLT immediate recall	11.67 (5.35)	14.99 (6.14)	**0.001[c]**

Sex (male %)	**AD (N = 94)**	**Non-AD (N = 99)**	***p value***
	28 (29.8%)	**31 (31.3%)**	**0.941[a]**
AVLT short-term delayed recall	2.63 (2.51)	4.85 (3.05)	**< 0.001[c]**
AVLT long-term delayed recall	1.81 (2.47)	4.38 (3.11)	**< 0.001[c]**
AVLT recognition	17.51 (3.32)	20.12 (3.08)	**< 0.001[c]**
Information processing speed			
SDMT (s)	22.13 (12.89)	32.53 (13.97)	**< 0.001**[b]
TMT A	87.67 (66.65)	51.00 (28.29)	**< 0.001[c]**
Executive function			
TMT B	103.75 (43.81)	78.97 (51.80)	**< 0.001**[c]
Stroop-C(s)	118.10 (48.26)	94.53 (33.98)	**0.004[c]**
Language			
BNT	17.62 (4.67)	19.04 (4.93)	0.058[c]
VFT	10.13 (4.13)	12.29 (4.28)	**0.008[b]**
Visuospatial			
ROCF	20.98 (7.75)	25.18 (7.09)	**< 0.001**[c]
Brain iron			
BG iron (ppm)	0.03 (0.02)	0.02 (0.03)	**< 0.001**[c]
Cortical Volume			
TIV (cm^3)	1400.87 (135.90)	1420.72 (161.01)	0.490[b]
l_HIP (cm^3)	3.21 (0.59)	3.81 (0.55)	**< 0.001**[c]
r_HIP (cm^3)	2.98 (0.65)	3.67 (0.55)	**< 0.001**[b]

Abbreviations: pTau, phosphorylated tau; Aβ, amyloid-β; NfL, neurofilament light chain; MMSE, Mini-Mental State Examination; CDR, Clinical Dementia Rating; AVLT, Auditory Verbal Learning Test; SDMT, Symbol Digit Modalities Test; SBP, systolic blood pressure; DBP, diastolic blood pressure; MBP, mean blood pressure; TIV,Total intracranial volume; TMT A/B, Trail Making Test Part A/B; Stroop C, Stroop Color and Word Test Part C; BNT, Boston Naming Test; VFT, Verbal Fluency Test; ROCF, Rey–Osterrieth

Complex Figure Test; BG, basal ganglia; l/r, left/right hemisphere; HIP, hippocampus. Continuous variables are reported as mean (standard deviation). a Chi-square test; b Two-sample t-test; c Mann-Whitney Test.

3.2. Brain iron deposition and regional volume differences

Voxel-wise analysis revealed significantly increased iron deposition in the left basal ganglia region in AD individuals compared to Non-AD, cognitively unimpaired individuals, with combined voxel-wise $p < 0.001$ and extent threshold FWEc = 60 voxels, corresponding to cluster-pFWE < 0.05 (**Figure S1**). The significant cluster of 60 voxels had 95% locating in left putamen and 5% in left accumbens area, with peak MNI coordinates at x = -16.5, y = 12, z = -3. The AD group exhibited significantly elevated basal ganglia iron deposition (0.03 ± 0.02 vs 0.02 ± 0.03 ppm, $p < 0.001$) compared to the Non-AD group. Bilateral hippocampal volumes were significantly reduced in the AD group (left: 3.21 ± 0.59 vs 3.81 ± 0.55 cm^3, $p < 0.001$; right: 2.98 ± 0.65 vs 3.67 ± 0.55 cm^3, $p < 0.001$) (Table 1).

3.3. Correlation analysis results

Partial correlation analyses, controlling for age and sex, revealed significant relationships among basal ganglia iron accumulation, plasma biomarkers, brain volumes, and cognitive performance (Fig. 2A-C, **Table S2**). In the overall cohort, basal ganglia iron levels were positively correlated with plasma pTau217 concentration (r = 0.23, *pFDR* < 0.01). Conversely, basal ganglia iron demonstrated inverse associations with multiple cognitive domains, including global cognition (MMSE: r = -0.26, *pFDR* < 0.01), episodic memory (AVLT long-term delayed recall: r = -0.28, *pFDR* < 0.01), language function (VFT: r = -0.32, *pFDR* < 0.01), visuospatial abilities (ROCF: r = -0.21, *pFDR* < 0.05). Subgroup analyses revealed that in the Non-AD group, basal ganglia iron was significantly associated with verbal fluency performance (VFT: r = -0.39, *pFDR* < 0.01), whereas no significant association was observed in the AD group. Scatter plots depicting significant correlations between basal ganglia iron and cognitive/biomarker measures across groups are shown in **Figure S2.**

3.4. Subgroup and interaction analyses across AD clinical stages

To examine stage-specific associations, partial correlation analyses were conducted within each clinical subgroup after controlling for age and sex (Fig. 3A). The correlation patterns revealed progressive changes across the AD continuum. Three-dimensional surface plots illustrated the interrelationships among basal ganglia iron, pTau217, and hippocampal volumes across disease stages (Fig. 3B). The surfaces showed relatively gentle slopes in Non-AD and preclinical AD stages, steeper gradients in prodromal AD, and flattening patterns in AD dementia, indicating stage-dependent effects. Scatter plots stratified by disease stage revealed that the relationship between basal ganglia iron and hippocampal volumes was weakest in the Non-AD group, strengthened progressively through preclinical AD, reached the steepest negative slopes in prodromal AD, and then plateaued in AD dementia (Fig. 3C). This pattern

indicates that iron dysregulation plays a critical role in driving hippocampal neurodegeneration particularly during the prodromal phase, with diminishing incremental impact in advanced disease stages.

3.5. Interaction effects between iron level and disease stage

To further investigate the modifying role of iron accumulation, participants were stratified by iron level (low vs. high, median split) and disease stage. Line plots demonstrated significant interaction effects between iron level and disease stage on hippocampal volumes (left, right, and total) (Fig. 4A). Individuals with high iron exhibited lower hippocampal volumes compared to those with low iron in the Non-AD stage. A crossover occurred in the preclinical AD stage, where the high iron group showed larger volumes than the low iron group. From the prodromal AD stage through AD dementia, the high iron group demonstrated more pronounced progressive volume decline, resulting in consistently smaller hippocampal volumes than the low iron group across the entire disease trajectory. Scatter plots stratified by iron level revealed distinct patterns in the relationship between pTau217 and hippocampal volumes. Across all participants (Fig. 4B), although individuals with high basal ganglia iron started with lower baseline hippocampal volumes, the low iron group exhibited steeper negative slopes (left: β = -0.829; right: β = -0.906; total: β = -1.735) compared to the high iron group (left: β = -0.370; right: β = -0.510; total: β = -0.880). In the AD group (Fig. 4C), the low iron group similarly showed steeper slopes (left: β = -0.415; right: β = -0.468; total: β = -0.882,) than the high iron group (left: β = -0.182; right: β = -0.315; total: β = -0.497). Conversely, in the AD group (Fig. 4D), the pattern reversed, with the high iron group displaying steeper slopes despite starting with lower volumes. These complex interaction patterns indicate that the relationship between iron, tau pathology, and hippocampal atrophy varies depending on disease stage and tau burden.

3.6. Mediation analysis results

Mediation analyses revealed that basal ganglia iron significantly mediated the relationship between plasma pTau217 and hippocampal volumes (Fig. 5). For right hippocampal volume, the path from pTau217 to basal ganglia iron was significant (a = 0.012, $p = 0.001$), as was the path from basal ganglia iron to right hippocampal volume (b = -4.125, $p = 0.008$). The direct effect of pTau217 on right hippocampal volume remained significant (c' = -0.734, $p < 0.001$), with the total effect also significant (c = -0.784, $p < 0.001$). Similar mediation patterns were observed for left hippocampal volume (a = 0.012, $p = 0.001$; b = -4.323, $p = 0.004$; c' = -0.615, $p < 0.001$; c = -0.667, $p < 0.001$). The indirect effect was significant for both outcomes (right hippocampus: $ab = -0.050$, 95% CI [− 0.107, − 0.010], $p = 0.039$, accounting for 6.4% of the total effect; left hippocampus: $ab = -0.053$, 95% CI [− 0.109, − 0.013], $p = 0.029$, accounting for 7.9% of the total effect), indicating partial mediation. Full path coefficients, standard errors, bootstrap confidence intervals, and proportions mediated are reported in **Table S3**.

3.7. Sensitivity of the findings to the plasma pTau217 cutoff

Because group assignment relied on a single, previously published plasma pTau217 threshold, we examined how sensitive the group differences were to this choice. Plasma pTau217 was right-skewed in this cohort (median 0.229 pg/mL, IQR 0.129–0.618, skewness 1.82), and the published cutoff of 0.242 pg/mL fell close to the sample median; only 3 participants (1.55%) lay within ± 0.005 pg/mL and 25 (12.95%) within ± 0.050 pg/mL of the threshold, indicating that few participants occupied the gray zone in which group assignment would be most vulnerable to measurement error (**Table S4**). At the published cutoff, all group differences were significant under both parametric and non-parametric testing, with a moderate effect size for basal ganglia iron (Cohen's d = 0.575, 95% CI [0.287, 0.863]) and large effect sizes for left, right, and total hippocampal volume (d = − 1.065, − 1.147, and − 1.133, respectively; all p < 0.001) (**Table S5**). Scanning 91 candidate cutoffs across the observed pTau217 range showed that the group difference in basal ganglia iron remained significant at 81.3% of candidate thresholds, and the differences in left, right, and total hippocampal volume at 98.9%, 100%, and 98.9% of thresholds, respectively; non-significant values occurred only at the extremes of the scan, where one group contained as few as 10 participants (**Tables S6 and S7**; **Figure S3**). The direction and approximate magnitude of all effects were therefore stable across the plausible range of thresholds, indicating that the findings are not an artifact of the particular cutoff adopted.

Discussion

The present study provides novel evidence for associations linking plasma pTau217, brain iron homeostasis, hippocampal neurodegeneration, and cognitive decline in Alzheimer's disease. Our principal findings demonstrate that: (1) AD individuals exhibit significantly elevated basal ganglia iron deposition and reduced hippocampal volumes; (2) the relationship between iron accumulation and hippocampal atrophy shows systematic stage-dependent variation, with the strongest association in prodromal AD; (3) iron levels modulate vulnerability to pTau217-related neurodegeneration, with high-iron and low-iron subgroups displaying distinct patterns; and (4) basal ganglia iron significantly mediates the relationship between plasma pTau217 and hippocampal atrophy. These findings position brain iron dysregulation as a critical, stage-dependent intermediate mechanism in the tau-neurodegeneration cascade.

Basal ganglia iron deposition was significantly elevated in AD individuals and increased progressively across AD stages, extending previous neuroimaging findings linking iron accumulation to AD pathology[27]. The basal ganglia represent a preferential site of age-related iron accumulation due to their high metabolic demands, dense dopaminergic innervation, and critical role in motor and cognitive functions[4]. In AD, this physiological iron deposition appears to be exacerbated through multiple tau-related mechanisms. Hyperphosphorylated tau disrupts axonal transport, impairing trafficking of iron-containing proteins and promoting focal iron retention[11, 28]. Additionally, tau pathology compromises

ferritin function and iron storage capacity, leading to increased labile iron pools that catalyze oxidative damage through Fenton chemistry[6, 29]. The significant correlation between plasma pTau217 and basal ganglia iron supports a direct relationship between peripheral tau burden and central iron dyshomeostasis, consistent with the hypothesis that systemic tau pathology drives regional iron accumulation in metabolically vulnerable brain regions[27, 30]. Consistent with the critical role of basal ganglia in cognition, iron levels in these regions correlated inversely with performance across multiple cognitive domains including global cognition, episodic memory, language function, and visuospatial abilities[31]. Iron-mediated dysfunction in cortico-striatal-thalamic circuits may contribute to these cognitive deficits through impaired dopaminergic neurotransmission, oxidative damage to myelinated fiber tracts, and propagation of dysfunction to hippocampal-cortical networks[32].

Stage-stratified correlation analyses revealed a particularly striking nonlinear pattern across the AD continuum. In Non-AD individuals and preclinical AD, the correlation strength between iron and hippocampal volumes was relatively modest. Critically, the prodromal AD stage exhibited the strongest negative correlation between basal ganglia iron and hippocampal volumes, indicating that this stage represents a period when iron dysregulation exerts its maximal neurodegenerative impact[12, 13]. This observation aligns with the conceptualization of prodromal AD as a transitional phase characterized by accelerated pathological progression and declining compensatory capacity[33]. At this juncture, pathological cascades including tau propagation, synaptic dysfunction, and neuroinflammation are fully activated, yet substantial neuronal populations remain viable and potentially salvageable[34]. Iron accumulation during this critical window may act as a catalyst that amplifies tau-mediated toxicity through generation of reactive oxygen species, promotion of tau hyperphosphorylation via activation of stress-responsive kinases such as GSK-3β and CDK5, and induction of ferroptosis[35]. In the dementia stage, these correlations plateau or weaken, suggesting that extensive neuronal loss may obscure further iron-atrophy relationships, or that surviving neurons have developed adaptive responses to chronic iron exposure[36, 37]. This stage-dependent pattern has critical therapeutic implications: interventions targeting iron homeostasis may yield maximal neuroprotective benefits when deployed during the prodromal phase, before irreversible neuronal loss occurs[38].

Individual differences in iron levels significantly modulated susceptibility to tau-mediated neurodegeneration. In Non-AD individuals, the high-iron subgroup displayed steeper slopes in the pTau217-hippocampus relationship compared to the low-iron subgroup, suggesting that even in the absence of significant tau pathology, elevated iron may render hippocampal neurons more vulnerable to early tau accumulation by creating a pro-oxidant cellular environment that sensitizes neurons to tau-induced stress[14]. Conversely, within AD individuals, the low-iron group showed steeper hippocampal volume declines with increasing pTau217 levels compared to the high-iron group, despite the high-iron group maintaining consistently smaller volumes throughout the disease trajectory. This pattern likely reflects that individuals with long-standing iron elevation have developed adaptive cellular responses including upregulation of antioxidant systems, enhanced ferritin expression, and compensatory alterations in iron-handling proteins that partially buffer against acute tau-iron synergistic toxicity, while the high-iron subgroup may also represent a distinct endophenotype with primary iron dysregulation that

drives early hippocampal vulnerability independent of tau, and a survivor bias may operate where individuals with both high iron and high tau burden rapidly progressed to dementia[39]. These complex interaction patterns underscore the importance of considering individual iron homeostasis profiles when predicting disease trajectories and designing personalized intervention strategies, with iron-targeted therapies tailored based on iron status[40].

The mediation analysis revealed that basal ganglia iron partially mediated the pTau217-hippocampal atrophy relationship. Tau pathology exerts neurodegenerative effects partially through iron-dependent pathways rather than solely through direct tau toxicity. Iron-catalyzed oxidative stress generates reactive oxygen species that damage lipid membranes, proteins, and DNA, creating a toxic cellular environment that accelerates neuronal dysfunction[35, 41]. Excess iron triggers ferroptosis, an iron-dependent form of regulated cell death characterized by lipid peroxidation and glutathione depletion, which contributes substantially to neuronal loss in AD[42]. The basal ganglia's extensive connectivity with hippocampal-cortical circuits may facilitate propagation of iron-induced damage to medial temporal structures through disruption of trophic support, compromise of synaptic integrity along cortico-striatal-hippocampal pathways, and promotion of transsynaptic tau spread[18]. Importantly, the persistence of a significant direct effect of pTau217 on hippocampal volume indicates that iron accumulation represents one of multiple parallel pathways through which tau drives neurodegeneration, consistent with the multifactorial nature of AD pathophysiology[43]. The observed inverse correlations between basal ganglia iron and multiple cognitive domains further suggest that iron exerts broad functional impacts through both direct subcortical mechanisms and hippocampal-mediated pathways, reinforcing its significance as a transdiagnostic therapeutic target.

Several limitations warrant consideration. First, the cross-sectional design precludes causal inference regarding the temporal sequence of iron accumulation, tau pathology, and hippocampal atrophy; longitudinal studies with repeated QSM assessments are needed to establish directionality. Second, our single-center sample may limit generalizability to populations with different genetic backgrounds and vascular risk profiles, and multi-site validation is warranted. Third, the small number of biomarker-positive participants in the preclinical AD stage, reflecting the challenges in recruiting this clinically silent population, may have limited the power of stage-specific analyses. Fourth, residual confounding from unmeasured variables including APOE genotype, inflammatory markers, and genetic variants influencing iron metabolism cannot be excluded. Future research should prioritize longitudinal studies, multi-site validation across diverse populations, and clinical trials evaluating iron-modulating interventions in staged and iron-stratified AD populations.

Conclusion

This study demonstrates that basal ganglia iron accumulation partially mediates the association between plasma pTau217 and hippocampal neurodegeneration in AD, suggesting that iron dysregulation could play an intermediate role in the tau–neurodegeneration cascade. The stage-dependent nature of this relationship, with iron exerting its maximal neurodegenerative impact during the prodromal phase

before extensive irreversible neuronal loss has occurred, underscores the importance of disease-stage stratification in future therapeutic trials targeting iron homeostasis. Individual differences in iron burden further modulate vulnerability to tau-mediated hippocampal atrophy, highlighting the potential value of iron profiling for personalized intervention strategies. These findings support the integration of plasma pTau217 measurement with QSM-based iron quantification as a complementary multimodal approach for improved patient stratification and risk assessment in AD.

Declarations

Authors' contributions

Pengbo Gao, and Haoye Tan contributed equally to data analysis, image processing, data interpretation, and manuscript writing. Guangshi Li, Jinxia Liang, Mingfeng Yang, and Danyan Xu participated in image processing and statistical analysis. Qiang Wang, Shuang Liang, Zhidai Xiao, Xiaomin Zheng, Yujiing Gan, Qixuan Chen, Mingyong Zeng and Weilin Wang were primarily responsible for data collection. Ben Chen, Xiaomei Zhong, and Yuping Ning provided the theoretical framework for this work, designed the experimental approach, supervised the study, and provided critical review and suggestions. All authors have read and approved the final manuscript.

Acknowledgments

We express our deepest gratitude to all participants and their families for their invaluable contributions to this study. We extend our sincere appreciation to the clinical and research staff at the Affiliated Brain Hospital of Guangzhou Medical University for their dedicated support and expertise throughout the conduct of this work.

Conflicts of Interest

The authors declare that they have no conflicts of interests.

Funding sources

The study was supported by National Natural Science Foundation of China (No. 82371428; No. 82471547); Guangdong Province Key Areas Research and Development Programs-Brain Science and Brain-Inspired Intelligence Technology (2023B0303010003); Natural Science Foundation of Guangdong Province, China (2024A1515011035、2025A1515011872、2026A1515012121); Brain Science and Brain-Like Intelligence Technology (2021ZD0201800); Guangzhou Science and Technology Plan Project (2025A03J3521); Guangzhou Key Clinical Specialty (Clinical Medical Research Institute); Guangzhou Municipal Key Discipline in Medicine (2025-2027).

Consent Statement

All participants or their legal guardians provided signed informed consent to participate in the study. The study adhered to the Declaration of Helsinki and was approved by the Affiliated Brain Hospital Ethics Committees of Guangzhou Medical University. Clinical data from the Affiliated Brain Hospital of Guangzhou Medical University are available from the corresponding author upon reasonable request.

Data available statement

The data that support the findings of this study are available from the corresponding author upon reasonable request.

References

1. Palmqvist S, et al. Discriminative Accuracy of Plasma Phospho-tau217 for Alzheimer Disease vs Other Neurodegenerative Disorders. JAMA. 2020;324(8):772–81.
2. Ashton NJ, et al. Plasma p-tau231: a new biomarker for incipient Alzheimer's disease pathology. Acta Neuropathol. 2021;141(5):709–24.
3. Janelidze S, et al. Plasma P-tau181 in Alzheimer's disease: relationship to other biomarkers, differential diagnosis, neuropathology and longitudinal progression to Alzheimer's dementia. Nat Med. 2020;26(3):379–86.
4. Zecca L, et al. Iron, brain ageing and neurodegenerative disorders. Nat Rev Neurosci. 2004;5(11):863–73.
5. Ayton S, et al. Regional brain iron associated with deterioration in Alzheimer's disease: A large cohort study and theoretical significance. Alzheimers Dement. 2021;17(7):1244–56.
6. Bulk M, et al. Postmortem MRI and histology demonstrate differential iron accumulation and cortical myelin organization in early- and late-onset Alzheimer's disease. Neurobiol Aging. 2018;62:231–42.
7. Haber SN, Fudge JL, McFarland NR. Striatonigrostriatal pathways in primates form an ascending spiral from the shell to the dorsolateral striatum. J Neurosci. 2000;20(6):2369–82.
8. Spotorno N, et al. Relationship between cortical iron and tau aggregation in Alzheimer's disease. Brain. 2020;143(5):1341–9.
9. Yan N, Zhang J. Iron Metabolism, Ferroptosis, and the Links With Alzheimer's Disease. Front Neurosci. 2019;13:1443.
10. Hambright WS, et al. Ablation of ferroptosis regulator glutathione peroxidase 4 in forebrain neurons promotes cognitive impairment and neurodegeneration. Redox Biol. 2017;12:8–17.
11. Lei P, et al. Tau deficiency induces parkinsonism with dementia by impairing APP-mediated iron export. Nat Med. 2012;18(2):291–5.

12. Jack CR Jr., et al. Tracking pathophysiological processes in Alzheimer's disease: an updated hypothetical model of dynamic biomarkers. Lancet Neurol. 2013;12(2):207–16.
13. Villemagne VL, et al. Amyloid beta deposition, neurodegeneration, and cognitive decline in sporadic Alzheimer's disease: a prospective cohort study. Lancet Neurol. 2013;12(4):357–67.
14. Bartzokis G, et al. Brain ferritin iron may influence age- and gender-related risks of neurodegeneration. Neurobiol Aging. 2007;28(3):414–23.
15. Henneman WJ, et al. Hippocampal atrophy rates in Alzheimer disease: added value over whole brain volume measures. Neurology. 2009;72(11):999–1007.
16. La Joie R et al. Prospective longitudinal atrophy in Alzheimer's disease correlates with the intensity and topography of baseline tau-PET. Sci Transl Med, 2020. 12(524).
17. Cha J, et al. Neural Correlates of Aggression in Medication-Naive Children with ADHD: Multivariate Analysis of Morphometry and Tractography. Neuropsychopharmacology. 2015;40(7):1717–25.
18. Haber SN, Knutson B. The reward circuit: linking primate anatomy and human imaging. Neuropsychopharmacology. 2010;35(1):4–26.
19. Bulk M, et al. Quantitative comparison of different iron forms in the temporal cortex of Alzheimer patients and control subjects. Sci Rep. 2018;8(1):6898.
20. Sultana R, et al. Oxidative modification and down-regulation of Pin1 in Alzheimer's disease hippocampus: A redox proteomics analysis. Neurobiol Aging. 2006;27(7):918–25.
21. Petersen RC. Mild cognitive impairment as a diagnostic entity. J Intern Med. 2004;256(3):183–94.
22. Widiger TA, Hines A. The Diagnostic and Statistical Manual of Mental Disorders, Fifth Edition alternative model of personality disorder. Personal Disord. 2022;13(4):347–55.
23. Zhong X, et al. Plasma p-tau217 and p-tau217/Abeta1-42 are effective biomarkers for identifying CSF- and PET imaging-diagnosed Alzheimer's disease: Insights for research and clinical practice. Alzheimers Dement. 2025;21(2):e14536.
24. Aarsland D, et al. Prevalence of Alzheimer's disease pathology in the community. Nature. 2026;650(8100):182–6.
25. Gaser C et al. CAT: a computational anatomy toolbox for the analysis of structural MRI data. Gigascience, 2024. 13.
26. Rolls ET, et al. Automated anatomical labelling atlas 3. NeuroImage. 2020;206:116189.
27. Damulina A, et al. Cross-sectional and Longitudinal Assessment of Brain Iron Level in Alzheimer Disease Using 3-T MRI. Radiology. 2020;296(3):619–26.
28. Duce JA, et al. Iron-export ferroxidase activity of beta-amyloid precursor protein is inhibited by zinc in Alzheimer's disease. Cell. 2010;142(6):857–67.
29. Kenkhuis B, et al. Iron loading is a prominent feature of activated microglia in Alzheimer's disease patients. Acta Neuropathol Commun. 2021;9(1):27.
30. Ayton S, et al. Ferritin levels in the cerebrospinal fluid predict Alzheimer's disease outcomes and are regulated by APOE. Nat Commun. 2015;6:6760.

31. Acosta-Cabronero J, et al. In vivo quantitative susceptibility mapping (QSM) in Alzheimer's disease. PLoS ONE. 2013;8(11):e81093.
32. Grahn JA, Parkinson JA, Owen AM. The cognitive functions of the caudate nucleus. Prog Neurobiol. 2008;86(3):141–55.
33. Petersen RC, et al. Author response: Practice guideline update summary: Mild cognitive impairment: Report of the Guideline Development, Dissemination, and Implementation Subcommittee of the American Academy of Neurology. Neurology. 2018;91(8):373–4.
34. Scheltens P, et al. Alzheimer's disease. Lancet. 2021;397(10284):1577–90.
35. Lovell MA, et al. Copper, iron and zinc in Alzheimer's disease senile plaques. J Neurol Sci. 1998;158(1):47–52.
36. Ashraf A, et al. Iron dyshomeostasis, lipid peroxidation and perturbed expression of cystine/glutamate antiporter in Alzheimer's disease: Evidence of ferroptosis. Redox Biol. 2020;32:101494.
37. Rouault TA. Iron metabolism in the CNS: implications for neurodegenerative diseases. Nat Rev Neurosci. 2013;14(8):551–64.
38. Stockwell BR, et al. Ferroptosis: A Regulated Cell Death Nexus Linking Metabolism, Redox Biology, and Disease. Cell. 2017;171(2):273–85.
39. Ward RJ, et al. The role of iron in brain ageing and neurodegenerative disorders. Lancet Neurol. 2014;13(10):1045–60.
40. Belaidi AA, Bush AI. Iron neurochemistry in Alzheimer's disease and Parkinson's disease: targets for therapeutics. J Neurochem. 2016;139(Suppl 1):179–97.
41. Yamamoto A, et al. Iron (III) induces aggregation of hyperphosphorylated tau and its reduction to iron (II) reverses the aggregation: implications in the formation of neurofibrillary tangles of Alzheimer's disease. J Neurochem. 2002;82(5):1137–47.
42. Jakaria M, et al. Ferroptosis as a mechanism of neurodegeneration in Alzheimer's disease. J Neurochem. 2021;159(5):804–25.
43. Bloom GS. Amyloid-beta and tau: the trigger and bullet in Alzheimer disease pathogenesis. JAMA Neurol. 2014;71(4):505–8.

Figures

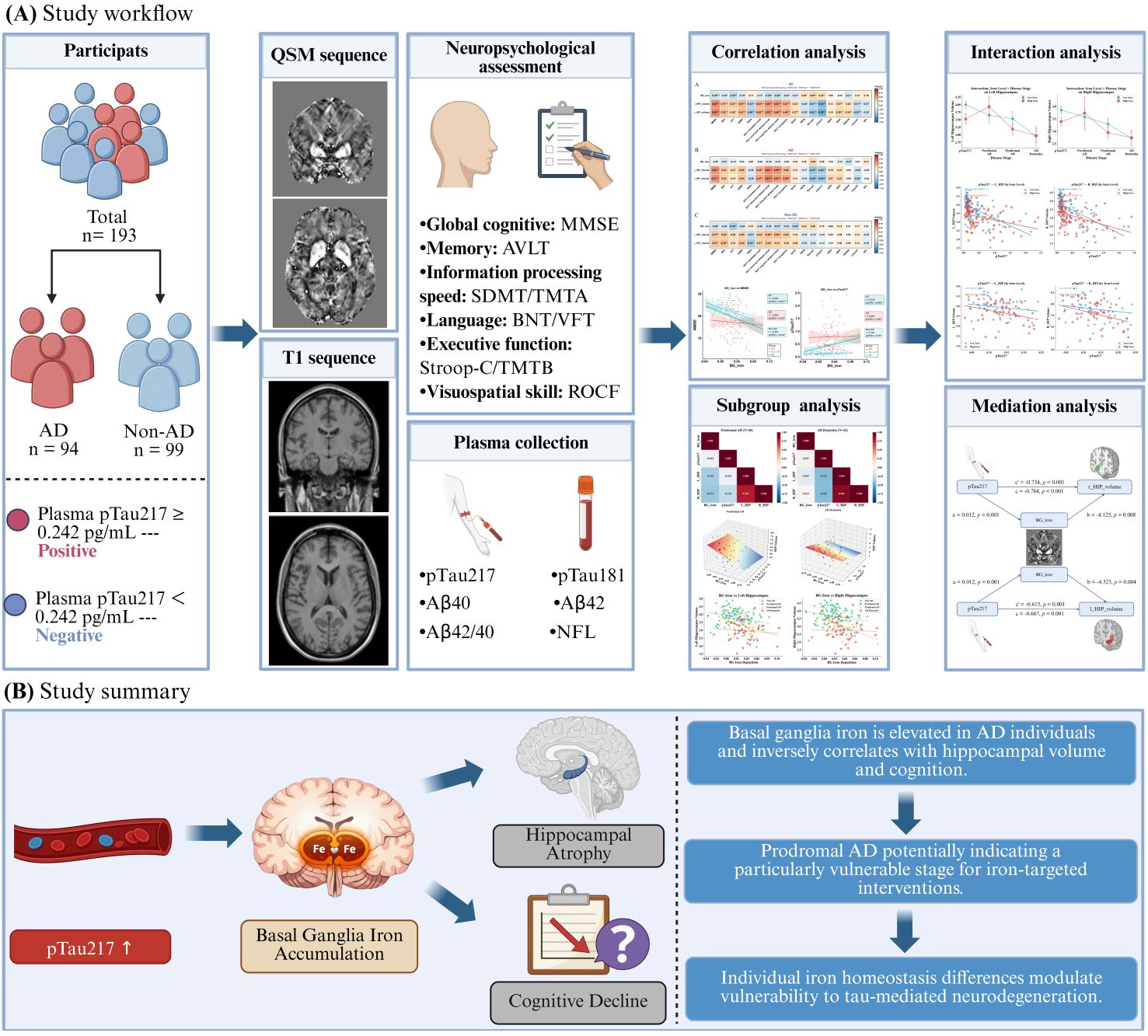


Figure 1

Study design and workflow. (A) A total of 193 participants were classified into AD (n = 94) and Non-AD (n = 99) groups based on plasma pTau217 concentration with a cutoff of 0.242 pg/mL. All participants underwent quantitative susceptibility mapping (QSM) and T1-weighted MRI scanning, comprehensive neuropsychological assessment, and plasma biomarker collection. Correlation, subgroup, interaction, and mediation analyses were performed to investigate relationships among plasma biomarkers, brain iron deposition, hippocampal volumes, and cognitive function. (B) The core conclusions of the study are summarized. **Abbreviations:** QSM, quantitative susceptibility mapping; MMSE, Mini-Mental State Examination; AVLT, Auditory Verbal Learning Test; SDMT, Symbol-Digit Modalities Test; TMTA/B, Trail Making Test Part A/B; BNT, Boston Naming Test; VFT, Verbal Fluency Test; ROCF, Rey-Osterrieth Complex

Figure Test; Aβ, amyloid-beta; NfL, neurofilament light chain; pTau, phosphorylated tau; BG, basal ganglia; HIP, hippocampus.

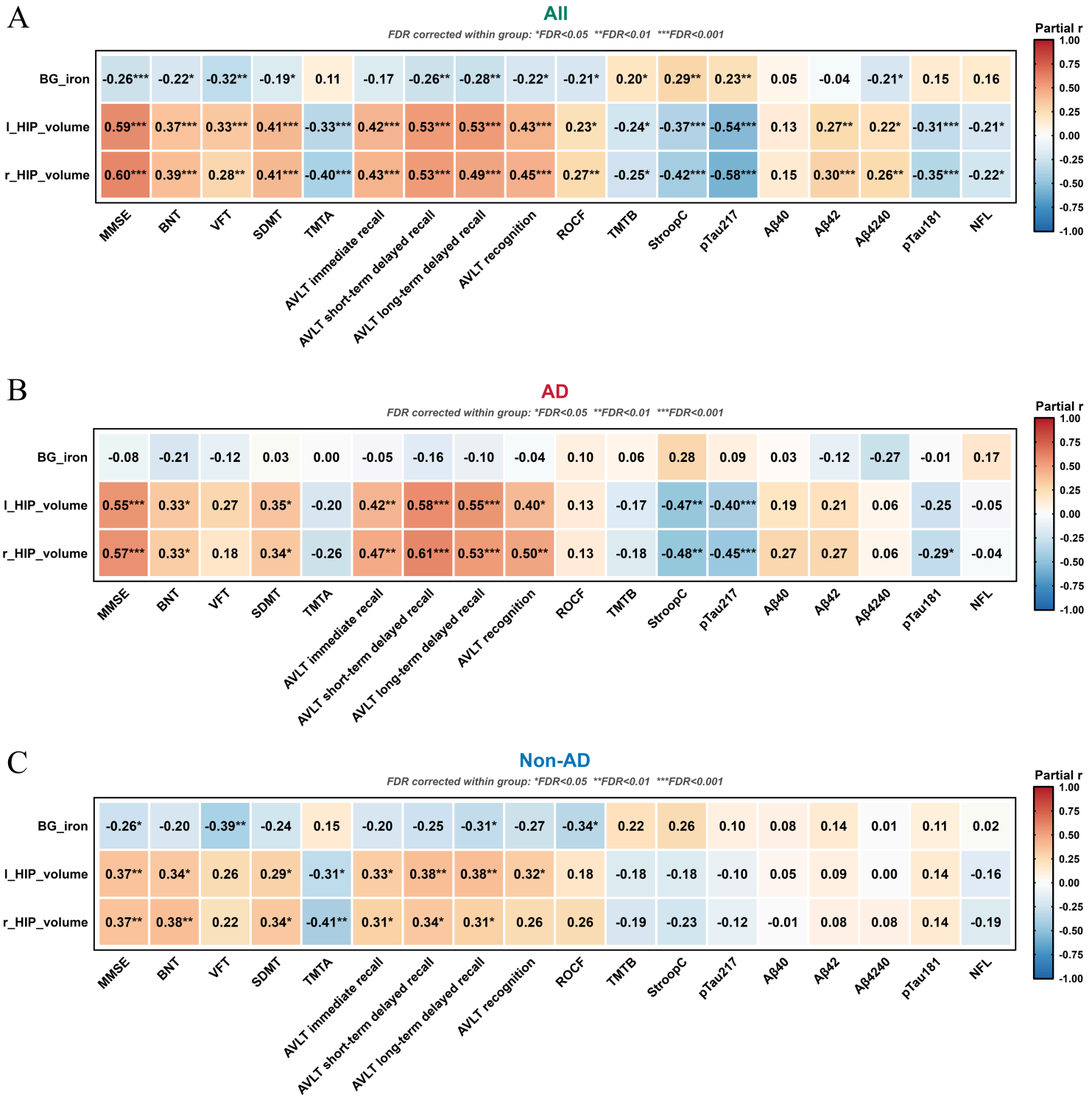


Figure 2

Correlation analyses between plasma biomarkers, brain iron, hippocampal volumes, and cognitive measures. (A-C) Heatmaps showing partial correlation coefficients in all participants (A), AD group (B), and Non-AD group (C). Asterisks indicate significance levels after FDR correction (*$pFDR$ < 0.05, **$pFDR$ <

0.01, ***pFDR* < 0.001). **Abbreviations:**NfL, neurofilament light chain; pTau, phosphorylated tau; MMSE, Mini-Mental State Examination; AVLT, Auditory Verbal Learning Test; TMTB, Trail Making Test Part B; VFT, Verbal Fluency Test; BNT, Boston Naming Test; ROCF, Rey-Osterrieth Complex Figure Test; BG_iron, basal ganglia iron; HIP, hippocampus; l, left; r, right; FDR, false discovery rate.

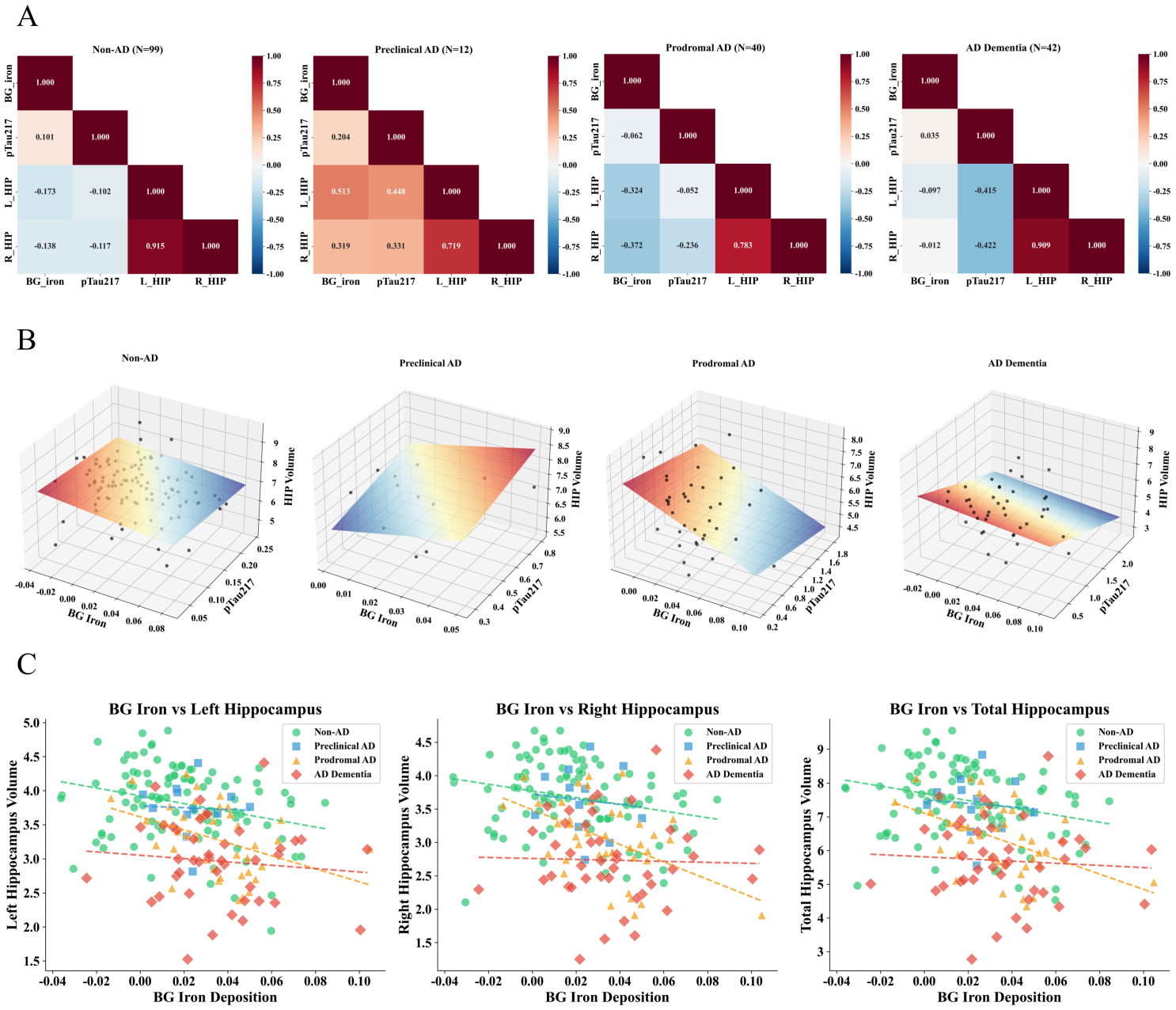


Figure 3

Subgroup and interaction analyses across AD clinical stages. (A) Heatmaps showing partial correlation coefficients within each clinical subgroup (Non-AD, preclinical AD, prodromal AD, and AD dementia). (B) Three-dimensional surface plots illustrating the relationships among basal ganglia iron, pTau217, and hippocampal volumes across different disease stages. (C) Scatter plots showing the relationship between basal ganglia iron and hippocampal volumes (left, right, and total) stratified by disease stage.

Abbreviations: AD, Alzheimer's disease; BG, basal ganglia; HIP, hippocampus; pTau217, phosphorylated tau 217; l, left; r, right.

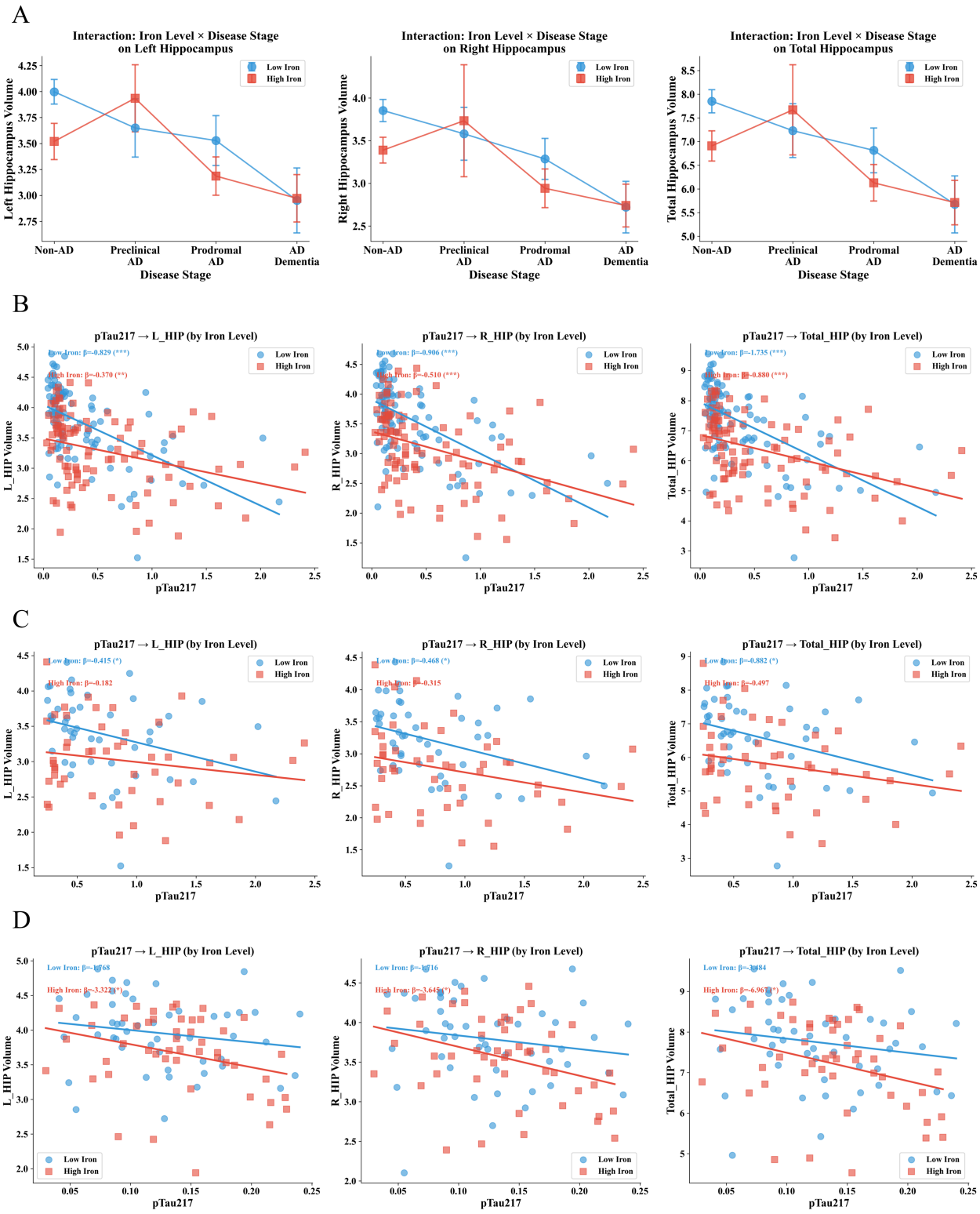


Figure 4

Interaction effects of iron level and disease stage on hippocampal volumes. (A) Line plots demonstrating the interaction between iron level (low vs. high, median split) and disease stage on left,

right, and total hippocampal volumes. Error bars represent standard errors. (B-D) Scatter plots showing the relationship between pTau217 and hippocampal volumes stratified by iron level across all participants (B), within the AD group stratified by clinical stage (C), and within the Non-AD group (D). Regression lines with 95% confidence intervals are shown for each iron level group. **Abbreviations:** AD, Alzheimer's disease; HIP, hippocampus; pTau217, phosphorylated tau 217; l, left; r, right.

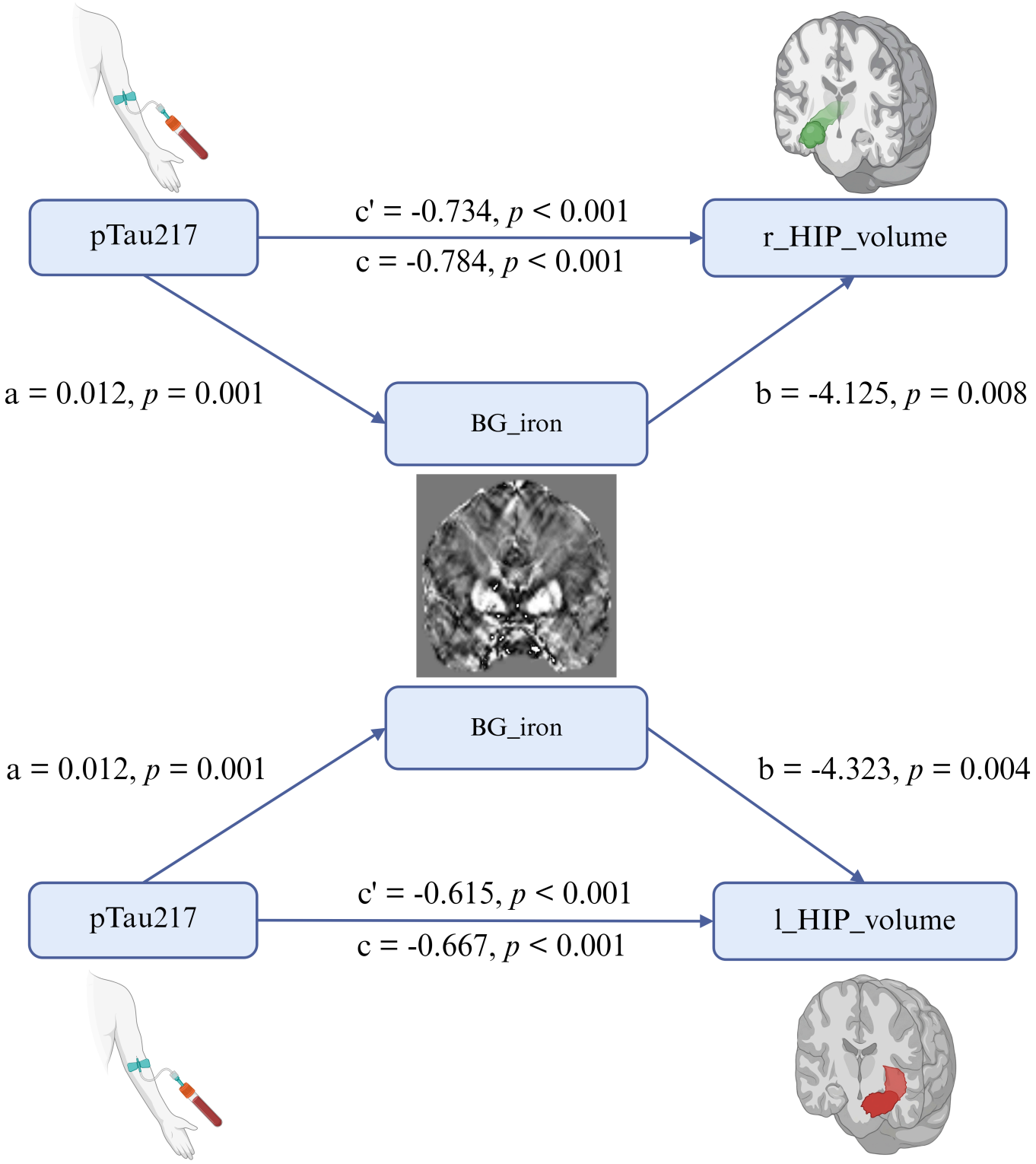


Figure 5

Mediation analyses. Basal ganglia iron (BG_iron) mediates the association between plasma pTau217 and bilateral hippocampal volumes. Upper panel: mediation model for right hippocampal volume (r_HIP_volume). Lower panel: mediation model for left hippocampal volume (l_HIP_volume).
Abbreviations: pTau217, phosphorylated tau 217; BG_iron, basal ganglia iron; r_HIP, right hippocampus; l_HIP, left hippocampus; MMSE, Mini-Mental State Examination; AMYG, amygdala; PHG, parahippocampal gyrus; r, right; l, left.

Supplementary Files

This is a list of supplementary files associated with this preprint. Click to download.

- Supplementarymaterial.docx
- FigureS1.png
- FigureS2.png
- FigureS3.png